Chinese Journal of Natural Medicines

Antimalarial and neuroprotective *ent*–abietane diterpenoids from the aerial parts of *Phlogacanthus curviflorus*

Jia LI, Xiao MENG, Chengyue YIN, Lixia ZHANG, Bin LIN, Peng LIU, Lingjuan ZHU, Haifeng WANG, Hongwei LIU, Xue ZHANG, Xinsheng YAO

Citation: Jia LI, Xiao MENG, Chengyue YIN, Lixia ZHANG, Bin LIN, Peng LIU, Lingjuan ZHU, Haifeng WANG, Hongwei LIU, Xue ZHANG, Xinsheng YAO, Antimalarial and neuroprotective *ent*–abietane diterpenoids from the aerial parts of *Phlogacanthus curviflorus*, Chinese Journal of Natural Medicines, 2023, 21(8), 619–630. doi: 10.1016/S1875–5364(23)60464–9.

View online: https://doi.org/10.1016/S1875–5364(23)60464–9

Available online at www.sciencedirect.com
ScienceDirect
Chinese Journal of Natural Medicines 2023, **21**(8): 619-630
doi: 10.1016/S1875-5364(23)60464-9
Chinese Journal of Natural Medicines

•Original article•

Antimalarial and neuroprotective *ent*-abietane diterpenoids from the aerial parts of *Phlogacanthus curviflorus*

LI Jia[1], MENG Xiao[1], YIN Chengyue[1], ZHANG Lixia[1], LIN Bin[2], LIU Peng[3], ZHU Lingjuan[1], WANG Haifeng[1], LIU Hongwei[4], ZHANG Xue[1*], YAO Xinsheng[1, 5*]

[1] *School of Traditional Chinese Materia Medica, Key Laboratory of Structure-Based Drug Design & Discovery of Ministry of Education, Shenyang Pharmaceutical University, Shenyang 110016, China;*
[2] *School of Pharmaceutical Engineering, Shenyang Pharmaceutical University, Shenyang 110016, China;*
[3] *School of Life Science and Biopharmaceutics, Shenyang Pharmaceutical University, Shenyang 110016, China;*
[4] *State Key Laboratory of Mycology, Institute of Microbiology, Chinese Academy of Sciences, Beijing 100101, China;*
[5] *Institute of Traditional Chinese Medicine & Natural Products, College of Pharmacy, Jinan University, Guangzhou 510632, China*

Available online 20 Aug., 2023

[ABSTRACT] Six new *ent*-abietane diterpenoids, abientaphlogatones A−F (**1**−**6**), along with two undescribed *ent*-abietane diterpenoid glucosides, abientaphlogasides A−B (**7**−**8**) and four known analogs were isolated from the aerial parts of *Phlogacanthus curviflorus* (*P. curviflorus*). The structures of these compounds were determined using high-resolution electrospray ionization mass spectrometry (HR-ESI-MS), one-dimensional and two-dimensional nuclear magnetic resonance (NMR) spectroscopy, electronic circular dichroism (ECD) spectra, and quantum chemical calculations. Notably, compounds **5** and **6** represented the first reported instances of *ent*-norabietane diterpenoids from the genus *Phlogacanthus*. In the *β*-hematin formation inhibition assay, compounds **2**, **4**, **7**−**10**, and **12** displayed antimalarial activity, with IC_{50} values of 12.97−65.01 μmol·L^{-1}. Furthermore, compounds **4**, **5**, **8**, and **10** demonstrated neuroprotective activity in PC12 cell injury models induced by H_2O_2 and MPP^+.

[KEY WORDS] *Phlogacanthus curviflorus*; Acathaceae; *ent*-Abietane diterpenoids; Antimalarial activity; Neuroprotective effect
[CLC Number] R284 **[Document code]** A **[Article ID]** 2095-6975(2023)08-0619-12

Introduction

The Dai medicine, one of the four national medicines in China, has evolved over thousands of years among the Dai people to address various health challenges, including disease prevention and treatment [1, 2]. In Dai-inhabited areas, the local climate, characterized by high temperatures and elevated humidity, contributes to the prevalence of common ailments such as malaria, cholera, and rheumatism [3-5]. The famous traditional Dai medicine "Huang Zhang", derived from the herbs of *Phlogacanthus curviflorus* (Wall.) Nees, is widely used for its therapeutic properties in heat-clearing and detoxification [6, 7]. *P. curviflorus*, belonging to the Acathaceae family, is distributed across Southeast Asia [8]. Extensive phytochemical investigations have revealed the presence of diterpenoids, iridoids, triterpenes, lignans, steroids, and flavonoids in the genus *Phlogacanthus* [9-12]. However, only two studies have explored the phytochemical composition of *P. curviflorus* roots, identifying *ent*-abietane diterpenoids as the primary constituents [9, 10]. While modern pharmacological investigations have demonstrated various bioactivities of *Phlogacanthus* species, including anti-oxidant [13-16], anti-diabetic [11, 17-19], anti-bacterial [15, 20, 21], anti-inflammatory [22], neuroprotective [23], cytotoxic [20, 24] and analgesic [22] activities, only the neuroprotective effect of *P. curviflorus* has been reported.

In our preliminary investigation, we evaluated the antimalarial potential of the 60% ethanol (EtOH) extract and its ethyl acetate soluble fraction obtained from the aerial parts of *P. curviflorus*. The *β*-hematin formation inhibition assay revealed inhibitory effects, with the extract and fraction displaying inhibition rates of 56.83% and 66.47% at a concentration of 100 μg·mL^{-1}, respectively. These findings, in conjunction with the traditional medicinal uses of Dai medicine, suggest the presence of antimalarial constituents in *P. curviflorus*. Therefore, systematic exploration was conducted to

[Received on] 16-Mar.-2023
[*Corresponding author] E-mails: syzxalice@163.com (ZHANG Xue); tyaoxs@jnu.edu.cn (YAO Xinsheng)
These authors have no conflict of interest to declare.

identify and investigate the chemical constituents responsible for the antimalarial activity within this plant. A total of 12 *ent*-abietane diterpenes were isolated and characterized, including eight previously unreported compounds (**1**−**8**) and four known compounds (**9**−**12**) (Fig. 1). *In vitro* antimalarial assays revealed varying degrees of activity for compounds **2**, **4**, **7**−**10**, and **12**. Furthermore, we assessed the neuroprotective effects of compounds **1**−**10** and **12** using PC12 cell injury models induced by H_2O_2 and MPP^+, respectively. Compounds **4**, **5**, **10** and **5**, **8**, **10** exhibited protective effects against H_2O_2-induced injury and MPP^+-induced injury in PC12 cells, respectively. Apart from phloantholide C, no reports have highlighted the presence of antimalarial and neuroprotective constituents within the genus *Phlogacanthus*. This paper provides a comprehensive account of the isolation, structural elucidation, as well as antimalarial and neuroprotective activities of the identified *ent*-abietane diterpenes.

Results and Discussion

Abientaphlogatone A (**1**) was isolated as a white amorphous powder. Its molecular formula was determined as $C_{20}H_{28}O_4$ with seven degrees of unsaturation, as deduced from the high-resolution electrospray ionization mass spectrometry (HR-ESI-MS) ion peak $[M + Na]^+$ at *m/z* 355.1867 (Calcd. for $C_{20}H_{28}O_4Na$, 355.1880). The ^1H nuclear magnetic resonance (NMR) spectroscopic data (Table 1) revealed distinctive signals, including an olefinic proton at δ_H 5.96 (1H, m, H-7), two oxymethines at δ_H 5.00 (1H, s, H-14) and 4.65 (1H, m, H-12), an oxygenated methylene at δ_H 3.80 (1H, d, J = 11.0 Hz, H-19a) and 3.43 (1H, d, J = 11.0 Hz, H-19b), and three methyls at δ_H 1.91 (3H, t, J = 1.8 Hz, H_3-17), 0.96 (3H, s, H_3-18) and 0.90 (3H, s, H_3-20). The analysis of the ^{13}C NMR and distortionless enhancement by polarization transfer (DEPT) spectra (Table 2) identified 20 carbon signals, comprising three methyls, six methylenes (one oxygenated), four sp^3 and one sp^2 methines (two oxygenated), two sp^3 and three sp^2 nonprotonated carbons, and a carbonyl carbon. These spectroscopic data combined with the heteronuclear multiple bond correlations (HMBC) (Fig. 2) of H-6/C-8, H-7/C-5, C-9, C-14, H-11/C-8, C-13, H-14/C-8, C-13, H_3-17/C-13, C-15, C-16, and H-19/C-3, C-4, C-18 indicated that compound **1** was a furan lactone-type *ent*-abietane diterpenoid with a double bond at C-7 and C-8 and two hydroxyl groups at C-14 and C-19, respectively. The relative configuration of compound **1**, except for C-14, was established based on the analysis of Nuclear Overhauser Effect Spectroscopy (NOESY) cross-peaks involving H-5/H_3-18, H-5/H-9, H-19a/H_3-20, and H_3-20/H-12 (Fig. 3). The relative configuration of C-14 was determined by comparing the chemical shift of C-14 (δ_C 69.9 in pyridine-d_5) under different orientations

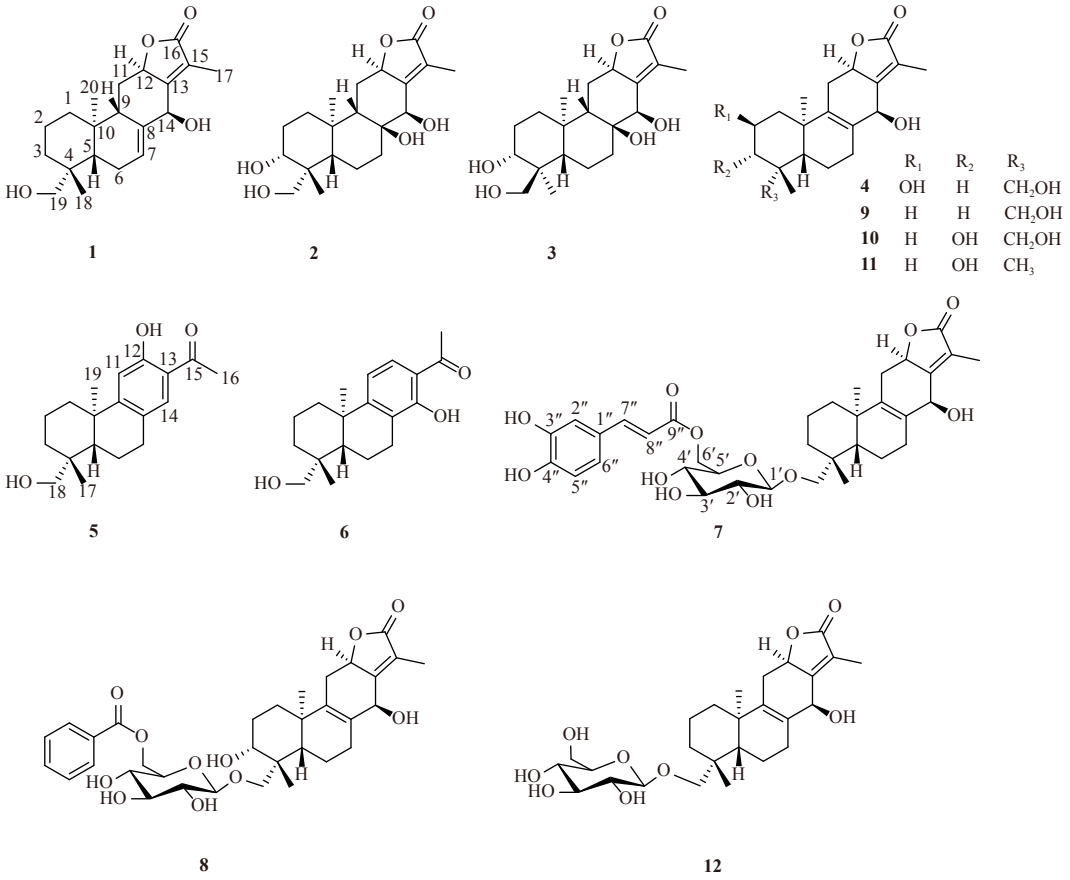

Fig. 1 Structures of compounds 1–12

Table 1 ^{1}H NMR (600 MHz) data for compounds 1–4 (*J* in Hz, in CD_3OD)

No.	1	2	3	4
1*α*	1.03 td (13.4, 3.7)	1.13 overlapped	1.11 m	0.98 t (11.6)
1*β*	1.90 overlapped	1.99 overlapped	1.98 m	2.07 overlapped
2*α*	1.47 m	1.75 m	1.69 overlapped	3.87 m
2*β*	1.58 m	1.80 m	1.70 overlapped	
3*α*	0.94 m	3.37 dd (11.7, 4.8)	3.64 m	0.86 t (12.2)
3*β*	1.93 overlapped			2.15 m
5	1.43 m	1.14 overlapped	1.45 dd (11.6, 1.0)	1.31 dd (12.6, 1.4)
6*α*	2.05 m	1.33 m	1.30 m	1.55 m
6*β*	2.22 m	1.73 m	1.55 m	1.93 dd (13.0, 7.5)
7*α*	5.96 m	1.27 m	1.36 m	2.04 overlapped
7*β*		2.63 dt (13.1, 2.5)	2.59 d (13.0)	2.45 m
9	2.43 m	1.62 m	1.65 overlapped	
11*α*	2.29 m	2.42 dd (13.3, 7.1)	2.43 m	2.93 dd (15.2, 6.7)
11*β*	1.50 m	1.66 m	1.65 overlapped	1.87 m
12	4.65 m	5.08 m	5.08 m	4.80 m
14	5.00 br s	4.75 d (1.3)	4.79 br s	4.96 br s
17	1.91 t (1.8)	1.99 t (1.7)	2.00 br s	1.98 t (1.8)
18	0.96 s	1.22 s	0.71 s	1.04 s
19	3.80 d (11.0)	4.07 d (11.2)	3.53 d (11.0)	3.65 d (11.2)
	3.43 d (11.0)	3.41 d (11.2)	3.28 d (11.0)	3.40 d (11.2)
20	0.90 s	1.03 s	1.08 s	1.08 s

Table 2 ^{13}C NMR (150 MHz) data for compounds 1–4 (in CD_3OD)

No.	1	2	3	4
1	40.0	40.2	40.2	45.8
2	19.3	28.5	27.8	65.1
3	36.5	80.6	73.1	45.2
4	39.0	43.8	43.4	41.1
5	51.9	57.0	48.3	53.1
6	24.3	20.6	19.8	19.4
7	129.8	37.8	37.0	30.1
8	137.1	78.8	78.9	131.2
9	45.9	57.3	57.3	138.2
10	37.4	39.5	39.5	40.7
11	28.1	29.8	29.8	33.5
12	80.2	80.1	80.2	79.7
13	166.2	164.8	164.9	163.6
14	70.8	72.3	72.4	70.8
15	123.8	123.6	123.5	121.9
16	177.4	177.6	177.6	177.4
17	9.1	9.3	9.3	9.1
18	27.4	24.0	13.3	27.8
19	64.7	65.0	66.8	65.8
20	14.6	19.7	19.7	20.7

of H-14 and H-12. When H-14 and H-12 exhibited the same orientation, the chemical shift of C-14 was observed at δ_C 69.9 in pyridine-d_5. When H-14 and H-12 showed the opposite orientation, the chemical shift of C-14 was observed at δ_C 64.9 in pyridine-d_5 [10]. Moreover, the DP4$^+$ probability analysis was employed to confirm the relative configuration of C-14 (Fig. 4). With a DP4$^+$ probability approaching 100%, the relative configuration of C-14 was assigned as 14*S**, aligning with the previously deduced configuration. The absolute configuration of compound **1** was determined as 4*R*, 5*S*, 9*S*, 10*R*, 12*R*, 14*S* by comparison of the calculated electronic circular dichroism (ECD) curve with the experimental ECD curve (Fig. 5). Thus, the structure of compound **1** was determined and designated as abientaphlogatone A.

Abientaphlogatone B (**2**) was obtained as a white amorphous powder. Its molecular formula was determined to be $C_{20}H_{30}O_6$ through HR-ESI-MS, with an observed ion peak $[M + Na]^+$ at *m/z* 389.1925 (Calcd. for $C_{20}H_{30}O_6Na$, 389.1935), indicating the presence of six degrees of unsaturation. Analysis of the ^{1}H NMR spectrum (Table 1) revealed the characteristic signals of three oxygenated methines at δ_H 5.08 (1H, m, H-12), 4.75 (1H, d, *J* = 1.3 Hz, H-14), and 3.37 (1H, dd, *J* = 11.7, 4.8 Hz, H-3), an oxygenated methylene at δ_H 4.07 (1H, d, *J* = 11.2 Hz, H-19a) and 3.41 (1H, d, *J* = 11.2 Hz, H-19b), and three methyls at δ_H 1.99 (3H, t, *J* = 1.7 Hz, H_3-17), 1.22 (3H, s, H_3-18), and 1.03 (3H, s, H_3-20). The ^{13}C NMR and DEPT data (Table 2) for compound **2** displayed 20

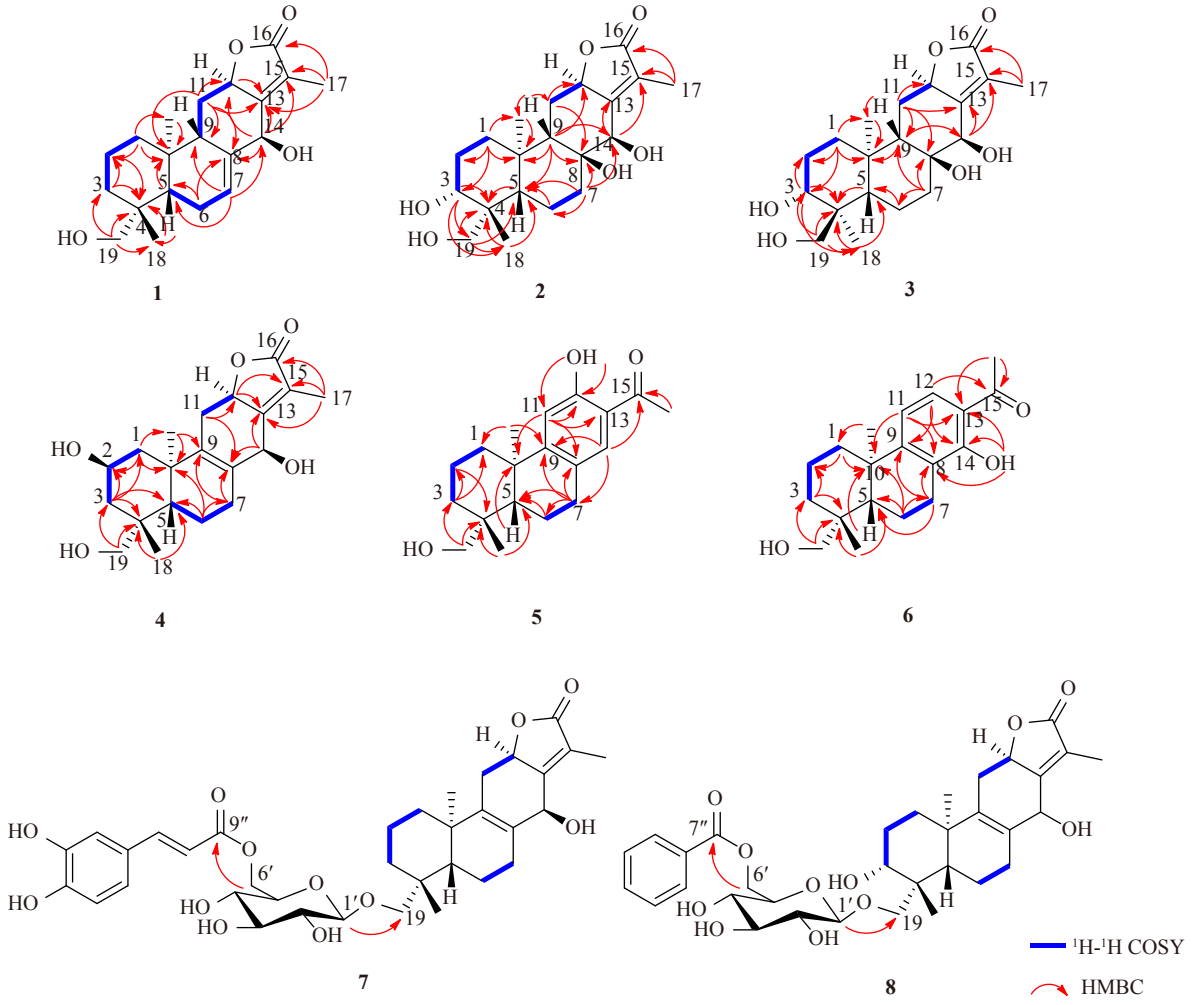

Fig. 2 Key ^{1}H-^{1}H COSY and HMBC correlations of compounds 1–8

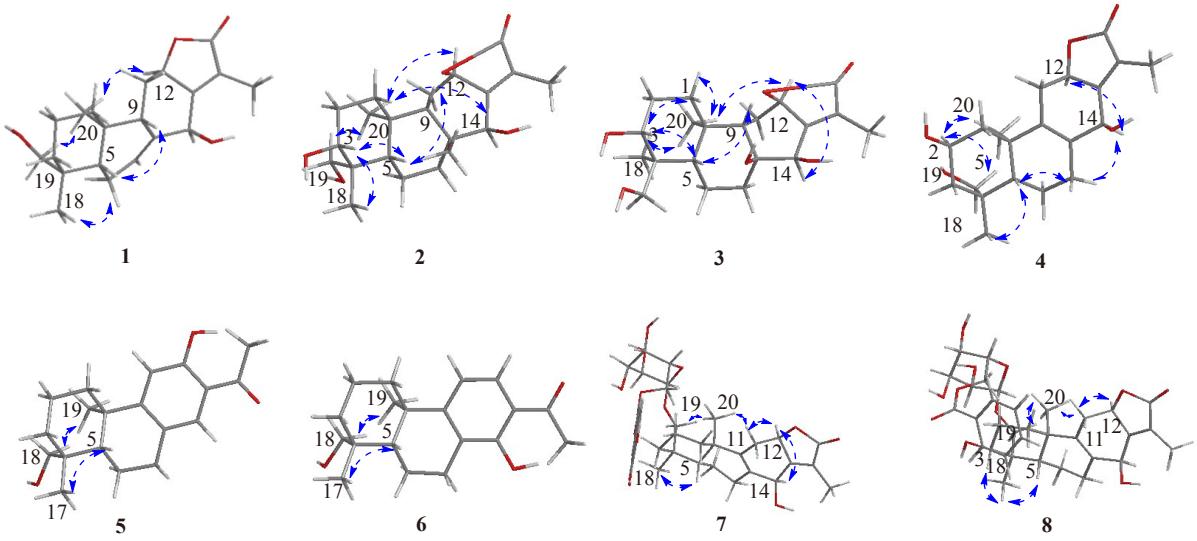

Fig. 3 NOESY correlations of compounds 1–8

carbon resonances, including three methyls, six methylenes (one oxygenated), five methines (three oxygenated), three sp^3 and two sp^2 nonprotonated carbons (one oxygenated), and a carbonyl carbon. Based on a comprehensive analysis of the ^{1}H-^{1}H correlated spectroscopy (COSY), heteronuclear single quantum correlation (HSQC), and heteronuclear multiple

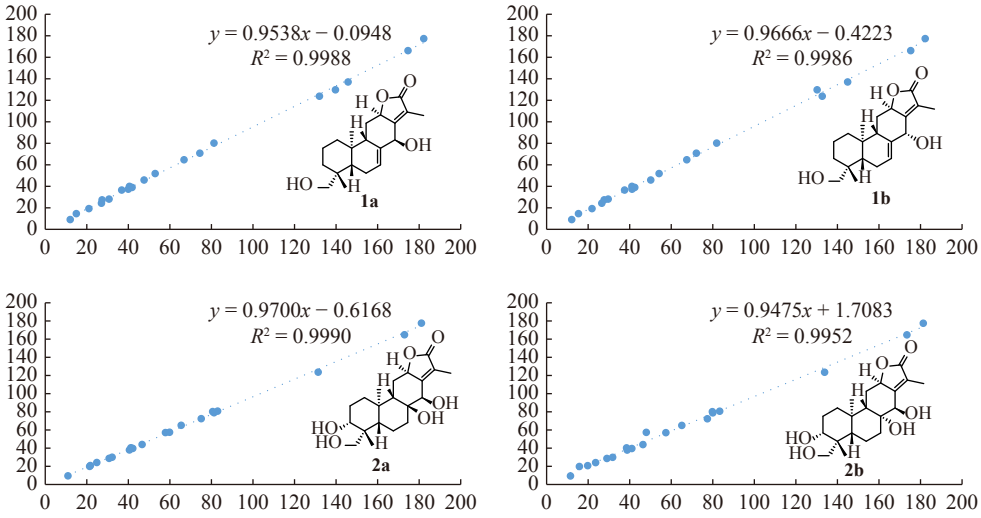

Fig. 4 Linear correlation between the experimental and calculated ^{13}C NMR chemical shifts and DP4$^+$ analysis of compounds 1 and 2

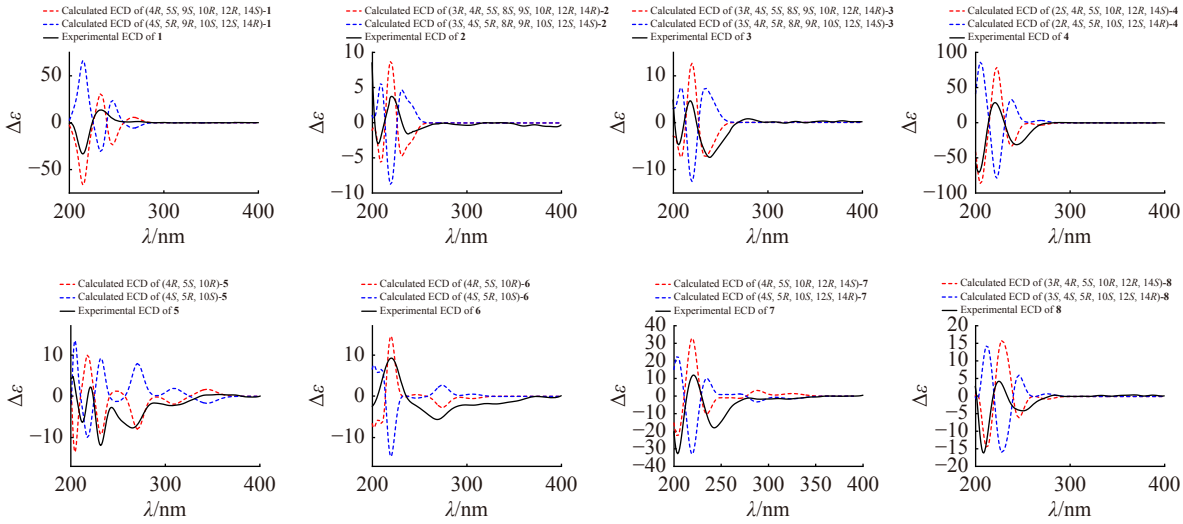

Fig. 5 Experimental and calculated ECD spectra of compounds 1−8

bond correlation (HMBC) spectra (Fig. 2) in conjunction with the molecular formula, compound **2** was identified as a furan lactone-type *ent*-abietane diterpenoid skeleton bearing four hydroxyl groups. The HMBC correlations (Fig. 2) of H-1/C-3, H-3/C-4, C-18, and C-19, H-7/C-8 and C-14, H-9/C-8 and C-14, H-14/C-13 and C-15, and H-19/C-3, C-4, C-5, and C-18 revealed that the four hydroxyl groups were positioned at C-3, C-8, C-14, and C-19 in compound **2**, respectively. Additionally, the NOESY correlations (Fig. 3) of H_3-20/H-12, H-14, H-19, H-3/H-5, H_3-18, and H-5/H-9 suggested the relative configuration of chiral carbons in the structure except for C-8. To determine the relative configuration of C-8, we performed computational analysis of the ^{13}C NMR data and DP4$^+$ probability analysis. The calculated result for **2a** [correlation coefficient (R^2) = 0.9990] exhibited a better fit with the experimental data than that for **2b** (R^2 = 0.9952) (Fig. 4). Moreover, the DP4$^+$ probability analysis assigned **2a** with a 100% probability (Fig. 4). To confirm the absolute configuration, ECD calculations were performed. A comparison between the experimental and calculated curves (Fig. 5) established the absolute configuration of compound **2** as 3*R*, 4*R*, 5*S*, 8*S*, 9*S*, 10*R*, 12*R*, 14*R*. Thus, the structure of compound **2** was elucidated and designated as abientaphlogatone B.

Abientaphlogatone C (**3**) was obtained as a white amorphous powder, sharing the same molecular formula as compound **2**, which was deduced from HR-ESI-MS with an ion at *m/z* 389.1922 [M + Na]$^+$ (Calcd. for $C_{20}H_{30}O_6Na$, 389.1935). Analyses of the 1D and 2D NMR spectra (Table 1, Table 2, Fig. 2) revealed an identical planar structure of compound **3** to that of compound **2**. However, a comparison of the ^{13}C NMR data between the two compounds highlighted differences at C-3, C-5, C-18, and C-19, which indicated that compound **3** was an epimer at C-4 in comparison

with compound **2**. This conclusion was further supported by the NOESY spectra (Fig. 3), which elucidated the relative configuration of compound **3**. The calculated ECD spectrum of (3*R*, 4*S*, 5*S*, 8*S*, 9*S*, 10*R*, 12*R*, 14*R*)-**3** demonstrated excellent agreement with the experimental ECD spectrum (Fig. 5), firmly establishing the absolute configuration of compound **3**. Consequently, compound **3** was designated as abientaphlogatone C.

Abientaphlogatone D (**4**), a white amorphous powder, exhibited a molecular formula of $C_{20}H_{28}O_5$, as determined by the HR-ESI-MS ion peak $[M + Na]^+$ at *m/z* 371.1824 (Calcd. for $C_{20}H_{28}O_5Na$, 371.1829). The ^1H and ^{13}C NMR spectroscopic data (Tables 1 and 2) for compound **4** were similar to those for compound **9**, with the exception of a methylene group being absent and the presence of an oxygenated methine in compound **4**. Crucial HMBC correlations (Fig. 2) of H-1 and H-3 with the oxygenated methine carbon at δ_C 65.1 evidenced the hydroxylation of C-2 in compound **4**. The relative configuration was assigned based on NOESY correlations (Fig. 3) of H-2/H-19 and H_3-20, H-14/H-7*α* and H-12, and H-5/H-7*β* and H_3-18. The absolute configuration of compound **4** was determined as 2*S*, 4*R*, 5*S*, 10*R*, 12*R*, 14*S* by comparing the calculated ECD spectrum with the experimental one (Fig. 5). Thus, the structure of compound **4** was established and named abientaphlogatone D.

Abientaphlogatone E (**5**) was obtained as a pale yellow powder. Its molecular formula was assigned as $C_{19}H_{26}O_3$ based on its HR-ESI-MS analysis (*m/z* 325.1783 $[M + Na]^+$; Calcd. for 325.1774). The ^1H NMR spectrum (Table 3) revealed a 1,2,4,5-tetrasubstituted benzene ring at δ_H 7.39 (1H, s, H-14) and 6.87 (1H, s, H-11), an oxygenated methylene at δ_H 3.84 (1H, d, *J* = 11.0 Hz, H-18a) and 3.56 (1H, d, *J* = 11.0 Hz, H-18b), and three methyls at δ_H 2.58 (3H, s, H_3-16), 1.18 (3H, s, H_3-19), and 1.07 (3H, s, H_3-17). The ^{13}C NMR and DEPT spectra (Table 3) of compound **5** exhibited 19 carbon resonances, including three methyls, six methylenes (one oxygenated), one sp^3 and two sp^2 methines, two sp^3 and four sp^2 nonprotonated carbons, and a carbonyl carbon. Compound **5** was confirmed to have the same planar structure and relative configuration as 12,19-dihydroxy-13-acetyl-8,11,13-podocarpatriene [25] based on the detailed analyses of ^1H-^1H COSY, HSQC, HMBC, and NOESY spectra (Figs. 2 and 3). However, a notable difference was observed in the specific rotation values between compound **5** $[[\alpha]_D^{20}$ −39.4 (*c* 0.1, CH_2Cl_2)] and 12,19-dihydroxy-13-acetyl-8,11,13-podocarpatriene $[[\alpha]_D^{15}$ +46.0 (*c* 0.14, CH_2Cl_2)], suggesting that compound **5** was the enantiomer of the above known compound. Additionally, the comparison of the calculated ECD spectrum and experimental ECD spectrum of compound **5** also confirmed its absolute configuration as 4*R*, 5*S*, 10*R*. Accordingly, compound **5** was identified as an *ent*-norabietane diterpenoid with an aromatized *C*-ring, and it was named abientaphlogatone E.

Abientaphlogatone F (**6**) was obtained as a pale yellow powder. Its molecular formula was determined to be $C_{19}H_{26}O_3$, which was identical with that of compound **5**, as deduced from the HR-ESI-MS analysis. A comparison of the ^1H NMR and ^{13}C NMR data (Table 3) for compound **6** with those for **5** revealed the substitution of a 1,2,4,5-tetrasubstituted benzene ring in compound **5** with a 1,2,3,4-tetrasubstituted benzene ring in compound **6**. This substitution was evidenced by the presence of ortho-coupled aromatic protons at δ_H 6.84 and 7.53 (each 1H, d, *J* = 8.7 Hz) in compound **6**. The assignment of this substitution was supported by the coupling constants (8.7 Hz) and HMBC correlations of 14-OH/C-8, C-13, and C-14, H-11/C-8, C-10, and C-13, and H-12/C-9, C-14, and C-15 (Fig. 2). The NOESY correlations (Fig. 3) of H-18/H_3-19 and H_3-17/H-5 suggested that 18-

Table 3 ^1H NMR (600 MHz) and ^{13}C NMR (150 MHz) data for compounds 5–6 (*J* in Hz, in $CDCl_3$)

No.	5		6	
	δ_H	δ_C	δ_H	δ_C
1*α*	1.42 m	38.6	1.39 m	38.5
1*β*	2.27 m		2.30 m	
2*α*	1.65 overlapped	18.8	1.63 overlapped	18.9
2*β*	1.72 overlapped		1.72 m	
3*α*	1.01 m	35.1	1.03 m	35.0
3*β*	1.89 m		1.90 m	
4		38.8		38.7
5	1.47 dd (12.8, 2.0)	50.6	1.46 overlapped	50.5
6*α*	1.69 overlapped	19.1	1.46 overlapped	18.2
6*β*	2.01 m		2.06 m	
7*α*	2.79 m	30.0	2.60 overlapped	24.4
7*β*	2.91 dd (16.4, 6.4)		2.94 dd (18.1, 6.3)	
8		125.8		124.6
9		159.6		158.5
10		38.5		38.4
11	6.87 s	133.8	6.84 d (8.7)	115.0
12		160.1	7.53 d (8.7)	127.6
13		117.9		116.1
14	7.39 s	131.0		160.7
15		203.9		204.1
16	2.58 s	26.5	2.59 s	26.5
17	1.07 s	26.8	1.07 s	26.8
18	3.84 d (11.0)	65.3	3.85 d (10.9)	65.2
	3.56 d (11.0)		3.57 d (10.9)	
19	1.18 s	25.3	1.19 s	25.0
12-OH	11.89 s			
14-OH			12.66 s	

CH_2OH and 19-CH_3 were in the *α*-orientation, and 17-CH_3 and H-5 were in the *β*-orientation. The absolute configuration of compound **6** was confirmed as 4*R*, 5*S*, 10*R* by comparing the experimental and calculated ECD spectra (Fig. 5). Based on these findings, the structure of compound **6** was elucidated and designated as abientaphlogatone F.

Abientaphlogaside A (**7**) was obtained as a yellow solid. Its molecular formula was determined as $C_{35}H_{44}O_{12}$ based on the $[M + Na]^+$ quasimolecular peak at *m/z* 679.2716 (Calcd. for $C_{35}H_{44}O_{12}Na$, 679.2725) observed in HR-ESI-MS analysis. The ^1H NMR and ^{13}C NMR data (Table 4) demonstrated that compound **7** was an *ent*-abietane diterpenoid with a caffeoyl group and a hexose unit. In-depth analyses of the ^1H-^1H COSY, HSQC, HMBC, and NOESY spectra (Figs. 2 and 3) displayed that the aglycone of compound **7** shared the same structure as compound **9**. The acid hydrolysis and high-performance liquid chromatography (HPLC) analysis, in combination with the coupling constant (J = 7.8 Hz) of the anomeric proton, confirmed the presence of *β*-D-glucose. The glucosidic linkage was established by the HMBC correlation (Fig. 2) between the anomeric proton of glucose at δ_H 4.18 (H-1') and C-19, providing evidence for the attachment of the glucosyl moiety to C-19. Additionally, the HMBC correlation between H-6' and the carbonyl carbon of the caffeoyl group at δ_C 169.0 revealed the acylation of the hydroxymethylene of the glucosyl moiety. The absolute configuration of compound **7** was finally validated by ECD calculations. The calculated ECD spectrum of (4*R*, 5*S*, 10*R*, 12*R*, 14*S*)-**7** (Fig. 5) exhibited good agreement with the experimental ECD spectrum. As a result, compound **7** was characterized as a new *ent*-abietane diterpenoid glucoside and named abientaphlogaside A.

Abientaphlogaside B (**8**), a yellow solid, was found to have a molecular formula of $C_{33}H_{42}O_{11}$ based on the HR-ESI-MS data (*m/z* 637.2610, $[M + Na]^+$). The ^1H NMR and ^{13}C NMR data (Table 4) demonstrated that compound **8** showed a similar *ent*-abietane diterpenoid glucoside structure to that of compound **7**. The difference between these two compounds lay in the presence of an additional hydroxyl group in the aglycone of compound **8**, with a benzoyl group in compound **8** replacing the caffeoyl group in compound **7**. HMBC correlations from the oxygenated methine proton at δ_H 3.79 to C-1, C-5, C-19, and from H_3-18 and H-19 to the oxygenated methine carbon at δ_C 70.7 indicated the hydroxylation of C-3, suggesting that the aglycone of compound **8** was euphelionolide M (**10**). The HMBC correlations of H-1'/C-19 and H-6'/C-7", in combination with the results of acid hydrolysis and HPLC analysis, confirmed the presence of D-glucose, where the hydroxymethylene was benzoylated. The coupling constant of the anomeric proton (J = 7.8 Hz) indicated a *β* configuration for the glycosyl moiety. The relative configuration of the *ent*-abietane diterpenoid skeleton, except for C-14, was determined by NOESY correlations (Fig. 3) of H_3-20/H-19a and H-11*α*, H-11*α*/H-12, and H_3-18/H-3 and H-5. Since the chemical shifts of C-14 in compounds **7** and **8** were

Table 4 ^1H NMR (600 MHz) and ^{13}C NMR (150 MHz) data for compounds 7–8 (J in Hz, in CD_3OD)

No.	7		8	
	δ_H	δ_C	δ_H	δ_C
1*α*	0.95 m	36.8	1.17 m	29.7
1*β*	1.60 overlapped		1.42 overlapped	
2*α*	1.36 overlapped	19.5	1.42 overlapped	26.3
2*β*	1.60 overlapped		1.84 m	
3*α*	0.82 m	36.5	3.79 m	70.7
3*β*	1.93 m			
4		39.0		43.2
5	1.21 dd (12.8, 1.0)	53.6	1.66 dd (12.8, 1.0)	46.3
6*α*	1.36 overlapped	19.4	1.42 overlapped	19.1
6*β*	1.84 m		1.76 overlapped	
7*α*	1.90 m	29.9	1.97 overlapped	29.9
7*β*	2.34 m		2.41 m	
8		130.8		130.9
9		138.6		138.6
10		39.4		38.9
11*α*	2.56 dd (15.4, 6.7)	33.3	2.68 dd (15.2, 6.6)	33.3
11*β*	1.68 m		1.76 overlapped	
12	4.60 m	79.9	4.72 m	79.8
13		163.9		163.9
14	4.86 overlapped	70.8	4.90 br s	70.8
15		121.7		121.8
16		177.6		177.4
17	1.96 t (1.7)	9.1	1.97 t (1.7)	9.1
18	1.00 s	27.6	1.08 s	22.9
19	4.03 d (9.5)	72.4	3.94 d (9.5)	73.6
	3.20 overlapped		3.34 overlapped	
20	0.86 s	20.1	0.76 s	19.7
1'	4.18 d (7.8)	104.4	4.22 d (7.8)	104.2
2'	3.20 overlapped	75.2	3.20 m	75.1
3'	3.35 m	78.3	3.34 overlapped	72.3
4'	3.26 t (9.5)	72.6	3.39 t (9.0)	78.2
5'	3.56 m	75.2	3.63 m	75.3
6'	4.43 overlapped	65.1	4.62 dd (11.8, 2.1)	65.7
	4.42 overlapped		4.50 dd (11.8, 7.4)	
1"		127.7		131.5
2"	7.04 d (2.0)	115.2	8.05 dd (8.2, 1.1)	130.8
3"		147.1	7.50 t (8.0)	129.7
4"		149.8	7.64 m	134.4
5"	6.79 d (8.2)	116.5	7.50 t (8.0)	129.7
6"	6.95 dd (8.2, 2.0)	123.3	8.05 dd (8.2, 1.1)	130.8
7"	7.56 d (15.8)	147.0		167.8
8"	6.27 d (15.8)	115.2		
9"		169.0		

identical (δ_C 70.8), the relative configuration of C-14 in compound **8** was deduced to be the same as that in compound **7**, which was also verified by the result of DP4$^+$ probability analysis (Fig. S80 in Supplementary material). Moreover, the calculated ECD spectrum of (3*R*, 4*R*, 5*S*, 10*R*, 12*R*, 14*S*)-**8** exhibited good agreement with the experimental ECD spectrum of **8** (Fig. 5). Therefore, the structure of compound **8** was determined and designated as abientaphlogaside B.

In addition, we isolated and identified four known compounds (**9**−**12**) (Fig. 1) through a rigorous analysis of their spectroscopic data, establishing their identity as phlogacantholide B (**9**) [10], euphelionolide M (**10**) [26], piscatolide (**11**) [27], and phlogacanthoside A (**12**) [10]. The comparison between our observed data and the reported spectroscopic data confirmed their structural similarity. It is worth noting that this is the first report of compounds **10** and **11** being discovered in the genus *Phlogacanthus*.

In an endeavor to identify potential antimalarial constituents from traditional Dai medicine, the antimalarial activity of all *ent*-abietane diterpenoids derived from the aerial parts of *P. curviflorus* was assessed through the *β*-hematin formation inhibition assay. Chloroquine diphosphate, a renowned antimalarial drug, was used as a positive control and exhibited an IC_{50} value of 8.53 ± 0.08 μmol·L^{-1}. As shown in Table 5, the results revealed that compounds **2**, **4**, **7**, and **10** could inhibit *β*-hematin formation with IC_{50} values of 12.97−22.85 μmol·L^{-1}, indicating their pronounced antimalarial activity. Furthermore, compounds **8**, **9**, and **12** exerted moderate inhibitory effects on *β*-hematin formation, suggesting their certain antimalarial activity. Intriguingly, compounds **5** and **6**, featuring the *ent*-norabietane diterpenoid skeleton and an aromatized *C*-ring, showed no activity, implying that the *C*-ring aromatization in *ent*-norabietane diterpenoids may not contribute to the antimalarial activity. Conversely, the presence of the furanolactone ring in *ent*-abietane diterpenoids appeared to be crucial for the *β*-hematin formation inhibition assay. Among the furan lactone-type *ent*-abietane diterpenoids, compound **1** with a double bond at C-7 and C-8, compound **3** with a 4*S* configuration, and compound **11** with two methyls substituted at C-4 demonstrated negligible activity. These findings suggest that the position of the double bond, the substituent group, and the configuration at C-4 may exert effects on the inhibitory activity against *β*-hematin formation. In addition, the glycosidation of 19-OH seems to have no impact on the inhibitory activity, as evidenced by the IC_{50} values of compounds **7**, **8**, and **12**. Further investigations are warranted to elucidate the underlying molecular mechanisms.

Furthermore, it is worth noting that phloantholide C, an *ent*-abietane diterpenoid isolated from *P. curviflorus*, has been previously documented for its neuroprotective properties [23]. To delve deeper into the potential neuroprotective effects of *ent*-abietane diterpenoids, we assessed all isolated compounds belonging to this class, excluding compound **11**, due to its limited availability. Resveratrol was included as a positive control in the experimental design. The evaluation

Table 5 Inhibitory activity of compounds 1−12 against *β*-hematin formation (mean ± SD, *n* = 3 for each group)

Compounds	IC_{50}/(μmol·L^{-1})
1	>100
2	22.85 ± 2.31
3	>100
4	14.21 ± 2.35
5	>100
6	>100
7	12.97 ± 1.14
8	62.67 ± 8.15
9	46.31 ± 2.66
10	17.80 ± 2.40
11	>100
12	65.01 ± 7.84
Chloroquine diphosphate	8.53 ± 0.08

encompassed the utilization of H_2O_2- and MPP$^+$-induced PC12 cell models. The cytotoxicity of **1**−**10** and **12** against PC12 cells was evaluated using the 3-(4,5-dimethylthiazol-2-yl)-2,5-diphenyltetrazolium bromide (MTT) assay. The concentrations resulting in a cell survival rate exceeding 80% were selected for subsequent neuroprotective evaluations (Table S7 in Supplementary material). As shown in Fig. 6A, compounds **5** and **10** could obviously attenuate the H_2O_2-induced injury in PC12 cells at 10 and 5 μmol·L^{-1}, respectively. Compound **4** could significantly alleviate PC12 cell injury induced by H_2O_2 at 20 and 50 μmol·L^{-1}. As shown in Fig. 6B, compounds **5**, **8**, and **10** could significantly enhance the viability of PC12 cells injured by MPP$^+$ at 10 μmol·L^{-1}. In the H_2O_2-induced PC12 cell injury model, compounds **4** and **10** significantly improved the cell viability, suggesting that the presence of the double bond at C-7 and C-8 and a hydroxyl group at C-2 or C-3 may be crucial in adjusting neuroprotective activities. In the MPP$^+$-induced PC12 cell injury model, a notable disparity in effects between compounds **7** and **8** was evident, indicating that the presence of benzoic acid fragment at C-6' of glucose may contribute to the augmented neuroprotection observed in *ent*-abietane diterpenoids. In both H_2O_2-induced and MPP$^+$-induced PC12 cell injury models, compound **5** consistently manifested significant neuroprotective effects, underscoring the potential significance of the hydroxyl group's positioning within *ent*-norabietane diterpenoids featuring an aromatized *C*-ring. However, it is essential to underscore that the aforementioned discussion serves as a preliminary analysis of the neuroprotective activity results and is confined to a limited range of compounds. Subsequent investigations are imperative to unravel the intricate structure-activity relationship underlying these phenomena.

Conclusions

This study presents a comprehensive investigation into

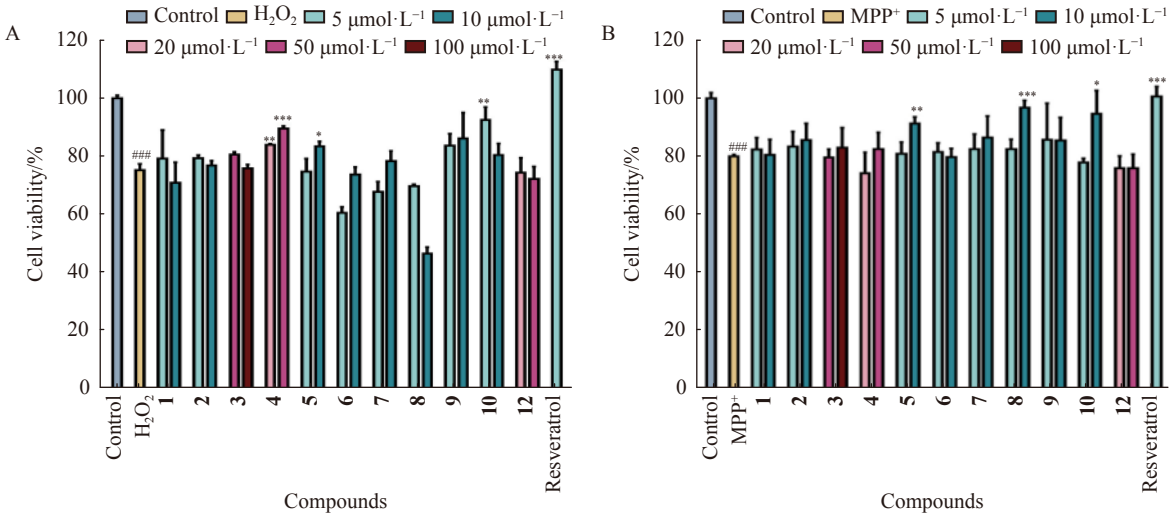

Fig. 6 The neuroprotective effects of compounds 1−10 and 12 in PC12 cells. A: Evaluation of the effect of 250 μmol·L^{-1} H_2O_2-induced injury. B: Evaluation of the effect of 500 μmol·L^{-1} MPP^+-induced injury. After H_2O_2 or MPP^+ treatment, cell viabilities are determined using the MTT assay in the presence or absence of the tested compounds at different concentrations. Data are expressed as mean ± SD (n = 3). $^*P < 0.05$, $^{**}P < 0.01$, $^{***}P < 0.001$ *vs* H_2O_2 or MPP^+-treated group; $^{\#\#\#}P < 0.001$ *vs* control

the chemical constituents of the antimalarial fraction derived from the aerial parts of *P. curviflorus*, well-known traditional Dai medicine called "Huang Zhang". Through systematic analysis, six previously unreported *ent*-abietane diterpenoids and two previously unreported *ent*-abietane diterpenoid glucosides, alongside four known analogs, were successfully isolated and characterized. Notably, the discovery of abientaphlogatones E and F (**5**−**6**) marks the first report of *ent*-norabietane diterpenoids within the genus *Phlogacanthus*. Furthermore, this study provides the inaugural evaluation of the antimalarial activity of constituents derived from the genus *Phlogacanthus*. In the *β*-hematin formation inhibition assay, compounds **2**, **4**, **7**−**10**, and **12** demonstrated varying degrees of antimalarial activity. Moreover, compounds **4**, **5**, **10** and **5**, **8**, **10** displayed noteworthy neuroprotective effects in PC12 cell injury models induced by H_2O_2 and MPP^+, respectively. This study sheds light on the previously unexplored neuroprotective potential of constituents from the genus *Phlogacanthus*, aside from the well-documented phloantholide C.

Materials and Methods

General experimental procedures

Ultraviolet (UV) spectra were recorded using a UV-2600i UV-visible spectrophotometer (Shimadzu, Kyoto, Japan). The ^1H, ^{13}C, and 2D NMR spectra were acquired using an AVANCE III HD spectrometer (Bruker, Bremen, Germany) equipped with a cryogenic probe (600 MHz). HR-ESI-MS data were obtained using a COMPACT Q-TOF/IT-TOF mass spectrometer (Bruker, Bremen, Germany). ECD spectra were measured on a MOS-450 (Bio-Logic Science, Grenoble, France). Optical rotations were determined using an MCP 200 polarimeter (Anton Paar GMBH, Graz, Austria). Column chromatography (CC) was performed using silica gel (100–200 and 200–300 mesh, Qingdao Marine Chemical Inc., Qingdao, China), Sephadex LH-20 (GE Healthcare, Uppsala, Sweden), and ODS (50 μm, YMC Company Ltd., Tokyo, Japan). The analytical HPLC was conducted using an Agilent 1200 system (CA, USA) equipped with a diode array detector and a reversed-phase C_{18} column (5 μm, 250 mm × 4.60 mm, Phenomenex Luna, CA, USA). Semi-preparative HPLC was performed using a Shimadzu LC-6AD instrument (Kyoto, Japan) equipped with a UV SPD-20A detector and a reversed-phase C_{18} column (5 μm, 250 mm × 10 mm, Phenomenex Luna, CA, USA).

Plant material

The aerial parts of *P. curviflorus* were collected from the Dehong Dai and Jingpo Autonomous Prefecture of Yunnan Province, China (GPS coordinates: 24°16' N/97°29' E) in November 2018. The plant material was authenticated by Professor WEI Songji (Guangxi University of Chinese Medicine, Guangxi, China). A voucher specimen (YLJPC-2018) was deposited at the School of Traditional Chinese Materia Medica, Shenyang Pharmaceutical University, China.

Extraction and isolation

The dried aerial parts of *P. curviflorus* (13.0 kg) were extracted with 60% EtOH (130 L × 2) for 2 h, resulting in a crude extract (1.8 kg). The crude extract was then suspended in H_2O (18.0 L) and partitioned sequentially with ethyl acetate (EtOAc; 18.0 L × 3) and *n*-butanol (*n*-BuOH; 18.0 L × 3). The EtOAc soluble fraction (170.0 g) was further purified using CC on silica gel eluted with cyclohexane : EtOAc (*V/V*, 99 : 1→60 : 40) and dichloromethane : methanol (CH_2Cl_2 : CH_3OH, *V/V*, 98 : 2→0 : 100). This purification process yielded fractions designated as Fr. YA−YR.

Fr. YF (4.6 g) was subjected to purification through a Sephadex LH-20 column (MeOH : CH_2Cl_2, 1 : 1, *V/V*) and an ODS column (MeOH : H_2O, *V/V*, 30%→80%). The 80%

MeOH eluate (58.1 mg) was further purified using semi-preparative HPLC (CH_3OH : H_2O, 73 : 27, *V/V*, 4 mL·min^{-1}), resulting in the isolation of compounds **5** (2.0 mg, t_R 13.8 min) and **6** (2.3 mg, t_R 18.3 min). Fr. YJ (4.8 g) was first subjected to purification using a Sephadex LH-20 column (MeOH : CH_2Cl_2, 1 : 1, *V/V*), followed by fractionation on an ODS column (MeOH : H_2O, *V/V*, 10%→60%), yielding fractions designated as Fr. YJ2A−YJ2J. Fr. YJ2H (409.0 mg) was further separated by semi-preparative HPLC (CH_3CN : H_2O, *V/V*, 25 : 75, 4 mL·min^{-1}), resulting in the isolation of compounds **1** (15.9 mg, t_R 22.1 min) and **9** (43.7 mg, t_R 28.3 min). Fr. YJ2I (98.8 mg) was purified using semi-preparative HPLC (CH_3CN : H_2O, *V/V*, 30 : 70, 4 mL·min^{-1}), yielding compound **11** (1.6 mg, t_R 18.0 min). Fr. YN (12.1 g) was separated on an ODS column (MeOH : H_2O, *V/V*, 10%→60%), leading to the isolation of fractions designated as Fr. YNA−YNO. Fr. YNE (205.6 mg) was further purified by semi-preparative HPLC (CH_3CN : H_2O, *V/V*, 10 : 90, 4 mL·min^{-1}), leading to the isolation of compounds **2** (9.0 mg, t_R 29.8 min) and **3** (3.6 mg, t_R 53.8 min). Compound **4** (20.4 mg, t_R 31.9 min) was obtained from Fr. YNF (1.5 g) through purification with semi-preparative HPLC (CH_3OH : H_2O, *V/V*, 30 : 70, 4 mL·min^{-1}). Fr. YNH (0.8 g) was subjected to purification on a Sephadex LH-20 column (MeOH : CH_2Cl_2, 1 : 1, *V/V*), yielding compound **10** (0.5 g). Fr. YO (29.6 g) was chromatographed on an ODS column (MeOH : H_2O, *V/V*, 30%→70%). The 40% MeOH eluate (12.7 g) was further purified by semi-preparative HPLC (CH_3OH : H_2O, *V/V*, 40 : 60, 4 mL·min^{-1}), resulting in the isolation of compound **12** (91.6 mg, t_R 42.5 min). Purification of the 50% MeOH eluate (6.4 g) by semi-preparative HPLC (CH_3CN : H_2O, *V/V*, 28 : 72, 4 mL·min^{-1}) resulted in the isolation of compounds **7** (12.3 mg, t_R 21.8 min) and **8** (2.1 mg, t_R 19.0 min).

Abientaphlogatone A (**1**) was obtained as a white amorphous powder. Its specific rotation was determined to be $[\alpha]_D^{20}$ −68.4 (*c* 0.5, MeOH). The UV spectrum of compound **1** dissolved in MeOH exhibited maximum absorption (λ_{max}) at 204 nm with a molar absorptivity (log ε) of 1.18 and at 220 nm with a log ε of 1.41. The infrared (IR) spectrum of compound **1**, measured using potassium bromide (KBr) as the matrix, showed characteristic absorption bands at ν_{max} 3446, 2964, 2933, 2850, 1749, 1631, 1444, 1385, 1036, and 1026 cm^{-1}. Its ECD spectrum in MeOH displayed λ_{max} ($\Delta\varepsilon$) values of 214 (−33.23) and 233 (+13.57) nm. The ^{1}H NMR (600 MHz, CD_3OD) and ^{13}C NMR (150 MHz, CD_3OD) data are presented in Tables 1 and 2. HR-ESI-MS analysis revealed the presence of $[M + Na]^+$ at mass-to-charge ratio (*m/z*) 355.1867 (Calcd. for $C_{20}H_{28}O_4Na$, 355.1880).

Abientaphlogatone B (**2**) was obtained as a white amorphous powder with a specific rotation of $[\alpha]_D^{20}$ −60.9 (*c* 0.9, MeOH). The UV spectrum in MeOH exhibited a λ_{max} (log ε) value of 220 (1.91) nm. The IR spectrum (KBr) showed characteristic absorption bands at ν_{max} 3475, 2974, 2931, 1695, 1662, 1450, 1356, 1146, 1026, and 1009 cm^{-1}. The ECD spectrum in MeOH displayed λ_{max} ($\Delta\varepsilon$) values of 207 (−2.94), 221 (+3.78), and 238 (−1.57) nm. ^{1}H NMR (600 MHz, CD_3OD) and ^{13}C NMR (150 MHz, CD_3OD) data are shown in Tables 1 and 2. HR-ESI-MS analysis revealed the presence of $[M + Na]^+$ at *m/z* 389.1925 (Calcd. for $C_{20}H_{30}O_6Na$, 389.1935).

Abientaphlogatone C (**3**) was obtained as a white amorphous powder with a specific rotation of $[\alpha]_D^{20}$ −51.2 (*c* 0.7 MeOH). In MeOH, the UV spectrum displayed a λ_{max} (log ε) value of 220 (1.11) nm, and the ECD spectrum showed characteristic absorption bands at λ_{max} ($\Delta\varepsilon$) values of 206 (−4.76), 218 (+4.62), and 239 (−7.46) nm. ^{1}H NMR (600 MHz, CD_3OD) and ^{13}C NMR (150 MHz, CD_3OD) data are depicted in Tables 1 and 2. HR-ESI-MS analysis unveiled the presence of $[M + Na]^+$ at *m/z* 389.1922 (Calcd. for $C_{20}H_{30}O_6Na$, 389.1935).

Abientaphlogatone D (**4**) was obtained as a white amorphous powder with a specific rotation of $[\alpha]_D^{20}$ −33.4 (*c* 0.1, MeOH). The UV spectrum in MeOH displayed a λ_{max} (log ε) value of 220 (2.88) nm. The IR spectrum (KBr) exhibited characteristic absorption bands at ν_{max} 3425, 2939, 1722, 1687, 1383, 1034, and 1022 cm^{-1}. The ECD spectrum in MeOH presented λ_{max} ($\Delta\varepsilon$) values of 204 (−70.06), 221 (+28.66), and 243 (−31.07) nm; ^{1}H NMR (600 MHz, CD_3OD) and ^{13}C NMR (150 MHz, CD_3OD) data are provided in Tables 1 and 2. HR-ESI-MS analysis uncovered the presence of $[M + Na]^+$ at *m/z* 371.1824 (Calcd. for $C_{20}H_{28}O_5Na$, 371.1829).

Abientaphlogatone E (**5**) was obtained as a pale yellow powder. Its specific rotation was $[\alpha]_D^{20}$ −39.4 (*c* 0.1, CH_2Cl_2). In MeOH, the UV spectrum exhibited λ_{max} (log ε) values of 203 (1.45) nm, 219 (1.44) nm, and 264 (0.87) nm, and the ECD spectrum exhibited λ_{max} ($\Delta\varepsilon$) values of 212 (−6.30), 220 (+2.24), 231 (−11.89), 243 (−2.69), 265 (−7.64), and 288 (−1.62) nm. ^{1}H NMR (600 MHz, CD_3OD) and ^{13}C NMR (150 MHz, CD_3OD) data are displayed in Table 3. HR-ESI-MS analysis revealed the presence of $[M + Na]^+$ at *m/z* 325.1783 (Calcd. for $C_{19}H_{26}O_3Na$, 325.1774).

Abientaphlogatone F (**6**) was obtained as a pale yellow powder with a specific rotation of $[\alpha]_D^{20}$ −42.7 (*c* 0.1, MeOH). In MeOH, the UV spectrum exhibited λ_{max} (log ε) values of 217 (1.71) nm and 268 (1.10) nm, and the ECD spectrum displayed λ_{max} ($\Delta\varepsilon$) values of 220 (+9.25) and 269 (−5.59) nm; ^{1}H NMR (600 MHz, CD_3OD) and ^{13}C NMR (150 MHz, CD_3OD) data are presented in Table 3. HR-ESI-MS analysis demonstrated the presence of $[M + Na]^+$ at *m/z* 325.1781 (Calcd. for $C_{19}H_{26}O_3Na$, 325.1774).

Abientaphlogaside A (**7**) was obtained as a yellow solid with a specific rotation of $[\alpha]_D^{20}$ −114.4 (*c* 0.4, MeOH). The UV spectrum in MeOH displayed λ_{max} (log ε) values of 206 (2.52) nm, 300 (0.90) nm, and 329 (1.07) nm. The IR spectrum (KBr) showed characteristic absorption bands at ν_{max} 3435, 2935, 1703, 1637, 1606, 1265, 1180, and 1165 cm^{-1}. The ECD spectrum in MeOH presented λ_{max} ($\Delta\varepsilon$) values of 204 (−32.72), 221 (+12.00), and 243 (−18.00) nm. ^{1}H NMR (600 MHz, CD_3OD) and ^{13}C NMR (150 MHz, CD_3OD) data

are provided in Table 4. HR-ESI-MS analysis uncovered the presence of $[M + Na]^+$ at *m/z* 679.2696 (Calcd. for $C_{35}H_{44}O_{12}Na$, 679.2725).

Abientaphlogaside B (**8**) was obtained as a yellow solid with a specific rotation of $[\alpha]_D^{20}$ −83.2 (*c* 0.4, MeOH). In MeOH, the UV spectrum displayed λ_{max} (log ε) values of 202 (1.12) nm and 224 (0.91) nm, and the ECD spectrum exhibited λ_{max} ($\Delta\varepsilon$) values of 204 (−16.08), 220 (+4.33), and 246 (−4.07) nm. ^{1}H NMR (600 MHz, CD_3OD) and ^{13}C NMR (150 MHz, CD_3OD) data are presented in Table 4; HR-ESI-MS analysis unveiled the presence of $[M + Na]^+$ at *m/z* 637.2590 (Calcd. for $C_{33}H_{42}O_{11}Na$, 637.2619).

NMR calculations

Geometry optimization of all conformers of compounds **1a/1b**, **2a/2b**, and **8a/8b** was performed using Gaussian 09 software at the B3LYP/6-31G(d) level in a methanol solvent model. Plausible conformers were further calculated at the B3LYP/6-311+G(d, p) level [28]. Subsequently, the calculated NMR data for these conformers were scaled based on the Boltzmann distribution theory. Finally, chemical shift errors were computed using linear regression and DP4$^+$ probability analysis [29].

ECD calculations

The absolute configurations of compounds **1**−**8** were determined using the Gaussian 09 program package. First, the compounds were constructed in GaussianView and subjected to a comprehensive conformational search using CONFLEX. Conformations with energies lower than 3.0 kcal·mol^{-1} were selected for subsequent calculations based on the density functional theory at the B3LYP/6-31G(d) level [30]. The ECD spectra of the selected conformers were then computed using at the B3LYP/6-311++G(2d, p) level, employing the CPCM solvation model in a MeOH solution. The calculated ECD curves were generated using SpecDis 1.51 and compared with the experimental ECD curves to determine their absolute configurations [31].

Acid hydrolysis and determination of sugars

For the acid hydrolysis and determination of sugars in compounds **7** and **8**, each compound (1.0 mg) was subjected to hydrolysis with 2 mol·L^{-1} HCl for 2 h at 90 °C. The resulting hydrolysate was dissolved in H_2O and extracted with $CHCl_3$. Subsequently, the aqueous layer was dried under vacuum to yield **7a** and **8a**. **7a**, **8a**, standard D-glucose and L-glucose (Sigma, St. Louis, MO, USA) were individually dissolved in 1.0 mL of pyridine containing L-cysteine methyl ester (3.0 mg, Sigma, St. Louis, MO, USA). The mixture was heated at 60 °C for 1 h, followed by the addition of otolyl isothiocyanate (5 μL, Sigma, St. Louis, MO, USA) and further heating at 60 °C for another 1 h. Finally, the resulting mixture was directly analyzed by HPLC on an RP-C_{18} column (5 μm, 4.60 mm × 250 mm; Phenomenex Luna, CA, USA) at 30 °C with isocratic elution (25% CH_3CN/0.1% formic acid, 0.8 mL·min^{-1}) [32]. The standard glucose derivatives exhibited single peaks at 20.250 min (D-glucose) and 18.390 min (L-glucose), respectively. The t_R for compounds **7** and **8** was 20.001 min and 19.899 min, respectively, confirming the presence of D-glucose.

β-Hematin formation inhibition assay

The *β*-hematin formation inhibition assay was conducted based on a previously reported method [33-35], with appropriate improvements. In a 96-well plate, 50 μL of tested samples at different concentrations in dimethyl sulfoxide (DMSO), 50 μL of hemin solution (1.0 mmol·L^{-1}, dissolved in 0.1 mol·L^{-1} NaOH solution, Sigma, St. Louis, MO, USA), and 80 μL of acetate buffer (4.0 mol·L^{-1}, pH 5.0) were added. The plate was then incubated at 55 °C for 5 h. Subsequently, the 96-well plate was cooled to room temperature, and 100 μL of a 30% (*V*/*V*) pyridine-HEPES solution (20.0 mmol·L^{-1}, pH 7.5, Sigma, St. Louis, MO, USA) was added to each well. After allowing for standing precipitation for 3 h, 25 μL of the supernatant was transferred to another 96-well plate, followed by the addition of 200 μL of pyridine-HEPES solution. The plate was thoroughly shaken, and the absorbance was measured at 405 nm. Chloroquine diphosphate (Sigma, St. Louis, MO, USA) served as a positive control, while DMSO was used as a negative control. All experiments were performed in triplicate.

Cell viability assay in PC12 cells induced by H_2O_2 and MPP$^+$

PC12 cells (ATCC, Manassas, VA, USA) were seeded in a 96-well plate at a density of 1 × 10^4 cells/mL and cultured in RPMI 1640 medium (Hyclone, Logan, USA) with 10% fetal bovine serum (FBS, Gibco, Gaithersburg, USA) in a humidified incubator at 37 °C and 5% CO_2 for 12 h. Subsequently, PC12 cells were exposed to 250 μmol·L^{-1} H_2O_2 or 500 μmol·L^{-1} MPP$^+$. After incubation for 12 h, the cells were added with tested compounds at various concentrations and incubated for another 12 h. Afterward, 10 μL of MTT (5 mg·mL^{-1}, Sigma, St. Louis, MO, USA) was added to each well. After 4 h of incubation, the medium was removed, and the formazan crystals were dissolved by DMSO. The absorbance of the formazan solution was measured at 490 nm (Bio-Rad Model 680, Bio-Rad, Hercules, CA, USA). In addition, cytotoxicity was evaluated by a colorimetric assay using the MTT method after the cells were incubated with the tested compounds for 24 h.

Supplementary material

UV, NMR, HR-ESI-MS, CD spectra and further detailed experimental information are available as Supplementary material, and can be requested by sending E-mails to the corresponding authors.

References

[1] Li MX, Ma YP, Zhang HX, *et al*. Repellent, larvicidal and adulticidal activities of essential oil from Dai medicinal plant *Zingiber cassumunar* against *Aedes albopictus* [J]. *Plant Divers*, 2021, **43**(4): 317-323.

[2] Duan BZ, Fang HL, Li XW, *et al*. Survey of traditional Dai medicine reveals species confusion and potential safety concerns: a case study on Radix Clerodendri Japonicum [J]. *Chin J Nat Med*, 2017, **15**(6): 417-426.

[3] Wen J, Qu Y, Li HY, *et al*. Survey of the correlation of the prevalence of G6PD deficiency and malaria in Xishuangbanna [J].

J Trop Med, 2006, **6**(9): 985-987.
[4] Liu AC, Li EK, Wu BQ, *et al*. Analysis of epidemic trend of class A and B infectious diseases in Dehong prefecture from 2011 to 2017 [J]. *China Health Stand Manage*, 2018, **9**(17): 5-8.
[5] Chen R, Kong CQ, He JL, *et al*. Characteristics and value of national medicine in Yunnan Province [J]. *China J Tradit Chin Med Pharm*, 2019, **34**(4): 1638-1640.
[6] *Chinese Materia Medica* [M]. Shanghai Scientific and Technical Publishers, 1999, **20**: 469.
[7] Zhou HH, Li JL, Chen LH, *et al*. Medication characteristics of Dai ethnomedicine in the treatment of bone diseases [J]. *Pharmacol Clin Chin Mater Med*, 2022, **38**(5): 169-174.
[8] Dutta B, Borthakur SK. A new variety of *Phlogacanthus curviflorus* (Wall.) Nees from Assam, India [J]. *Bangladesh J Plant Taxon*, 2016, **23**(1): 71-74.
[9] Lai GF, Wang XY, Wang YF, *et al*. Diterpenes and diterpene glucosides from *Phlogacanthus curviflorus* [J]. *Helv Chim Acta*, 2009, **92**: 470-480.
[10] Yuan XH, Li BG, Zhang XY, *et al*. Two diterpenes and three diterpene glucosides from *Phlogacanthus curviflorus* [J]. *J Nat Prod*, 2005, **68**(1): 86-89.
[11] Ahmed MDR, Sultana T, Routary R, *et al*. Chemistry and antidiabetic effects of *Phlogacanthus thyrsiflorus* Nees flowers [J]. *Nat Prod Chem Res*, 2016, **4**(5): 229-235.
[12] Barua AK, Biswas S, Patra A, *et al*. Phloganthoside: a diterpene lactone glucoside from *Phlogacanthus thyrsiflorus* [J]. *Phytochemistry*, 1987, **26**(2): 491-492.
[13] Boro H, Mashahary K, Das S. GC-MS analysis, phytochemicals and *in-vitro* antioxidant properties of root extracts of *Phlogacanthus thyrsiflorus* Nees, western Assam, India [J]. *Int J Pharm Sci Res*, 2019, **10**(6): 3012-3021.
[14] Suchiang K, Kayde NH. Comparative phytochemical analysis of *Phlogacanthus thyrsiflorus* Nees: implications of attenuation of pro-oxidants and pathogen virulence in *Caenorhabditis elegans* model system [J]. *Asian J Pharm Clin Res*, 2017, **10**(5): 361-367.
[15] Subba B, Sharma A, Budhathoki A. Assessment of phytochemical content, antioxidant and antibacterial activities of three medicinal plants of Nepal [J]. *J Med Plants Res*, 2016, **10**(45): 829-837.
[16] Laitonjam WS, Yumnam RS, Kongbrailatpam BD. Phytoconstituents of *Phlogacanthus pubinervius* Nees: leaves and their free radical scavenging activities [J]. *Nat Prod J*, 2012, **2**(4): 287-292.
[17] Bora J, Sahariah P, Patar AK, *et al*. Attenuation of diabetic hepatopathy in alloxan-induced diabetic mice by methanolic flower extract of *Phlogacanthus thyrsiflorus* Nees [J]. *J Appl Pharm Sci*, 2018, **8**(7): 114-120.
[18] Bora J, Syiem D, Bhan S. Methanolic flower extract of *Phlogacanthus thyrsiflorus* Nees attenuates diabetic nephropathy in alloxan-induced diabetic mice [J]. *Asian J Pharm Clin Res*, 2018, **11**(7): 113-116.
[19] Chakravarty S, Kalita JC. Role of the incretins in hypoglycemic effect of *Phlogacanthus thyrsiflorus* Nees in chemically induced diabetic mice [J]. *Int J Pharm Sci Res*, 2016, **7**(2): 646-659.
[20] Kumar A, Bidyapani T, Digvijay S, *et al*. Study of phytochemical compositions of leaves extracts of *Phlogacanthus thyrsiformis*, its antibacterial and silver nanoparticle derived cell cytotoxicity on HeLa cell line [J]. *J Pharm Res*, 2017, **11**(12): 1513-1517.
[21] Gogoi PK, Begum T, Borthakur B, *et al*. Green synthesis of silver nanoparticles using leaf extract of *Phlogacanthus thyrsiformis* and evaluation of their antibacterial and catalytic activity [J]. *Natl Acad Sci Lett*, 2015, **38**(3): 231-234.
[22] Das BK, Al-Amin MM, Chowdhury NN, *et al*. Analgesic, anti-inflammatory, and anti-oxidant activities of *Phlogacanthus thyrsiflorus* leaves [J]. *J Basic Clin Physiol Pharmacol*, 2015, **26**(2): 153-159.
[23] Meineck M, Schuck F, Abdelfatah S, *et al*. Identification of phlogacantholide C as a novel ADAM10 enhancer from traditional Chinese medicinal plants [J]. *Medicines*, 2016, **3**(4): 30-39.
[24] Tiwary BK, Bihani S, Kumar A, *et al*. The *in vitro* cytotoxic activity of ethno-pharmacological important plants of Darjeeling district of West Bengal against different human cancer cell lines [J]. *BMC Complement Altern Med*, 2015, **15**: 22-31.
[25] Gao YP, Shen YH, Xu XK, *et al*. Diterpenoids from *Gaultheria yunnanensis* [J]. *Phytochem Lett*, 2014, **8**: 6-9.
[26] Wang WP, Jiang K, Zhang P, *et al*. Highly oxygenated and structurally diverse diterpenoids from *Euphorbia helioscopia* [J]. *Phytochemistry*, 2018, **145**: 93-102.
[27] Reis MA, Paterna A, Mónico A, *et al*. Diterpenes from *Euphorbia piscatoria*: synergistic interaction of lathyranes with doxorubicin on resistant cancer cells [J]. *Planta Med*, 2014, **80**: 1739-1745.
[28] Michael WL, Matthew RS, Dean JT. Computational prediction of ^{1}H and ^{13}C chemical shifts: a useful tool for natural product, mechanistic, and synthetic organic chemistry [J]. *Chem Rev*, 2012, **112**: 1839-1862.
[29] Grimblat N, Zanardi MM, Sarotti AM. Beyond DP4: an improved probability for the stereochemical assignment of isomeric compounds using quantum chemical calculations of NMR Shifts [J]. *J Org Chem*, 2015, **80**: 12526-12534.
[30] Li J, Wang G, Qin Y, *et al*. Neuroprotective constituents from the aerial parts of *Cannabis sativa* L. subsp. sativa [J]. *RSC Adv*, 2020, **10**: 32043-32049.
[31] Bruhn T, Schaumlöffel A, Hemberger Y, *et al*. SpecDis: quantifying the comparison of calculated and experimental electronic circular dichroism spectra [J]. *Chirality*, 2013, **25**: 243-249.
[32] Tanaka T, Nakashima T, Ueda T, *et al*. Facile discrimination of aldose enantiomers by reversed-phase HPLC [J]. *Chem Pharm Bull*, 2007, **55**(6): 899-901.
[33] Shan H, Liu ZQ, Chen YZ, *et al*. Study on *β*-hematin formation inhibition activities of 24 common-used herbal medicines of Bai nationality [J]. *J Dali Univ*, 2016, **1**(10): 1-4.
[34] Xiao CJ, Xu W, Liu ZQ, *et al*. Evaluation of the antimalarial activity of 25 herbal medicines from west Yunnan [J]. *J Pathog Biol*, 2014, **9**(6): 542-545.
[35] Ncokazi KK, Egan TJ. A colorimetric high-throughput *β*-hematin inhibition screening assay for use in the search for antimalarial compounds [J]. *Anal Biochem*, 2005, **338**: 306-319.

Cite this article as: LI Jia, MENG Xiao, YIN Chengyue, ZHANG Lixia, LIN Bin, LIU Peng, ZHU Lingjuan, WANG Haifeng, LIU Hongwei, ZHANG Xue, YAO Xinsheng. Antimalarial and neuroprotective *ent*-abietane diterpenoids from the aerial parts of *Phlogacanthus curviflorus* [J]. *Chin J Nat Med*, 2023, **21**(8): 619-630.